NPL National Physical Laboratory

Report

NPL REPORT MAT 2

High-Frequency Vibration Tests of Sn-Pb and Lead-Free Solder Joints

D Di Maio and C Hunt

NOT RESTRICTED

AUGUST 2007

National Physical Laboratory | Hampton Road | Teddington | Middlesex | United Kingdom | TW11 0LW

Switchboard 020 8977 3222 | **NPL Helpline** 020 8943 6880 | **Fax** 020 8943 6458 | **www.npl.co.uk**

High-Frequency Vibration Tests of Sn-Pb and Lead-Free Solder Joints

Davide Di Maio and Christopher Hunt
Industry and Innovation Division

ABSTRACT

The introduction of lead-free alloys, driven by the European legislation Restriction on Harzardous Substances (RoHS), has revolutionised the electronic manufacturing market. New materials have replaced conventional SnPb alloy in a large number of applications and many more will follow. For this reason a better understanding of the properties of the new solder alloys in a broader range of applications is clearly needed. There are many applications in which electronics devices are subjected to vibration. Yet while there has been much research into the effects of low-cycle fatigue, there has been very little in the field of high-cycle fatigue, despite this being of interest in critical fields such as the aerospace industry. In consequence, this work has been aimed at studying lead-free solder alloys in a high-frequency environment, above 100 Hz, using SnPb alloy as a benchmark. Many previous studies on high-cycle fatigue have been focused on studying the effects on a full printed circuit board. That assessment method, however, is not suitable for characterising the solder performance, as the approach is geometry and condition specific.

In this work therefore, a more general approach has been adopted, using a reproducible model solder joint as the sample to which well controlled vibrations have been applied. The chosen frequencies for this research were 400 and 800 Hz, corresponding to an acceleration in the range of 10 to 20*g*. The lifetime of the joint was recorded, as well as the material properties' response to the vibration. This study highlighted the different behaviour of the various alloys when subjected to vibration, and in particular the superiority of the SnPb alloy, especially at higher frequencies. This method has been shown to be useful in characterising and ranking various materials, and tests could be easily repeated with a range of conditions, targeted at specific industrial applications. The results suggest that the higher the concentration of silver in the lead-free alloys, the better is the performance at 400 Hz. The method is versatile, and the equipment could easily be modified for testing at high temperatures.

ISSN 1754-2979

National Physical Laboratory
Hampton Road, Teddington, Middlesex, TW11 0LW

Approved on behalf of the Managing Director, NPL,
by Dr M G Cain, Knowledge Leader, Materials Team
authorised by Director, Industry and Innovation Division

CONTENTS

1 INTRODUCTION

A common failure mode in electronic devices is of a mechanical nature in which the interconnect fails i.e. ruptures/breaks [1]. It is estimated that although 80% of these electromechanical failures are related to thermal issues, about 20% are due to some form of vibration or shock. Electronic devices can be subjected to various forms of vibration, depending on the application and working environment. Vibration of the circuit board is transmitted from the system which can be fixed or moving, and arises for example from rotating and tumbling masses, from contact with rough surfaces (such as for vehicles), from engines, or from aerodynamic buffeting. These different sources generate vibrations that can be random or periodic, and extend over a wide range of frequencies and accelerations. They can be part of the application itself, such as in the use of ultrasonics, or they can be due to an occasional circumstance, such as the equipment being transported. This wide variety of sources and types of possible vibration experienced by electronic equipment, severely complicates any a study of the effect of the vibrations on the electronic components.

The structure and geometry of the system are important variables that affect any vibration of the circuit board. The type of components, where components are placed on the PCB, the type of PCB used, and even the features of the chassis will affect the magnitude of vibration at specific locations and the natural resonant frequencies. Vibrations at these resonant frequencies should be avoided to maintain low acceleration levels. Vibration test data show that most of the damage in electronic assemblies occurs at the fundamental natural frequency of the PCBs [1]. Vibration failures are normally the effect of high acceleration levels, high stress levels or large displacement amplitudes. The levels of these variables will depend on the application [1] - see Figure 1.

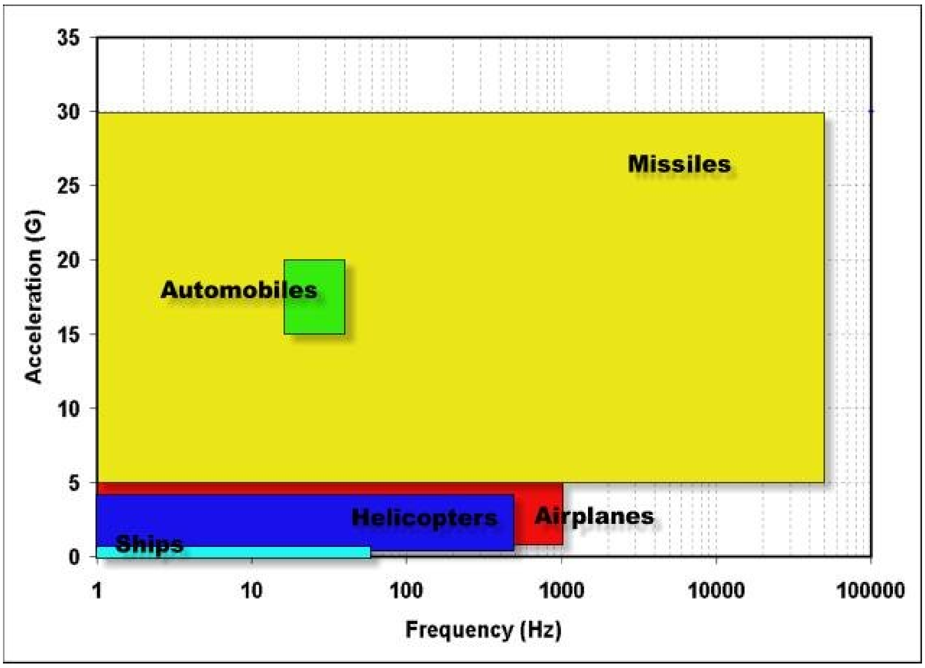

Figure 1: Acceleration/frequency graph for various applications.

Environmental conditions influence the fatigue life of electronic components. Temperature is particularly important, and solder joints are typically stressed at a high homologous temperature that facilitate creep, stress relaxation and microstructural changes. All these factors will affect the impact of vibration on any failure. The materials used for printed circuit boards (PCBs) and solder joints also play an important role in determining the fatigue life of the electronic device. PCBs are commonly made by laminating layers of glass-reinforced epoxy with layers of copper, and ribs are often added to increase stiffness. The ribs can be made of steel, aluminium or the same epoxy glass material. By stiffening the board the resonant frequency becomes higher. Sometimes damping strips, made of layers of viscoelastic materials, are added to the PCBs in order to reduce the dynamic displacement, the forces, and the stresses associated with vibration.

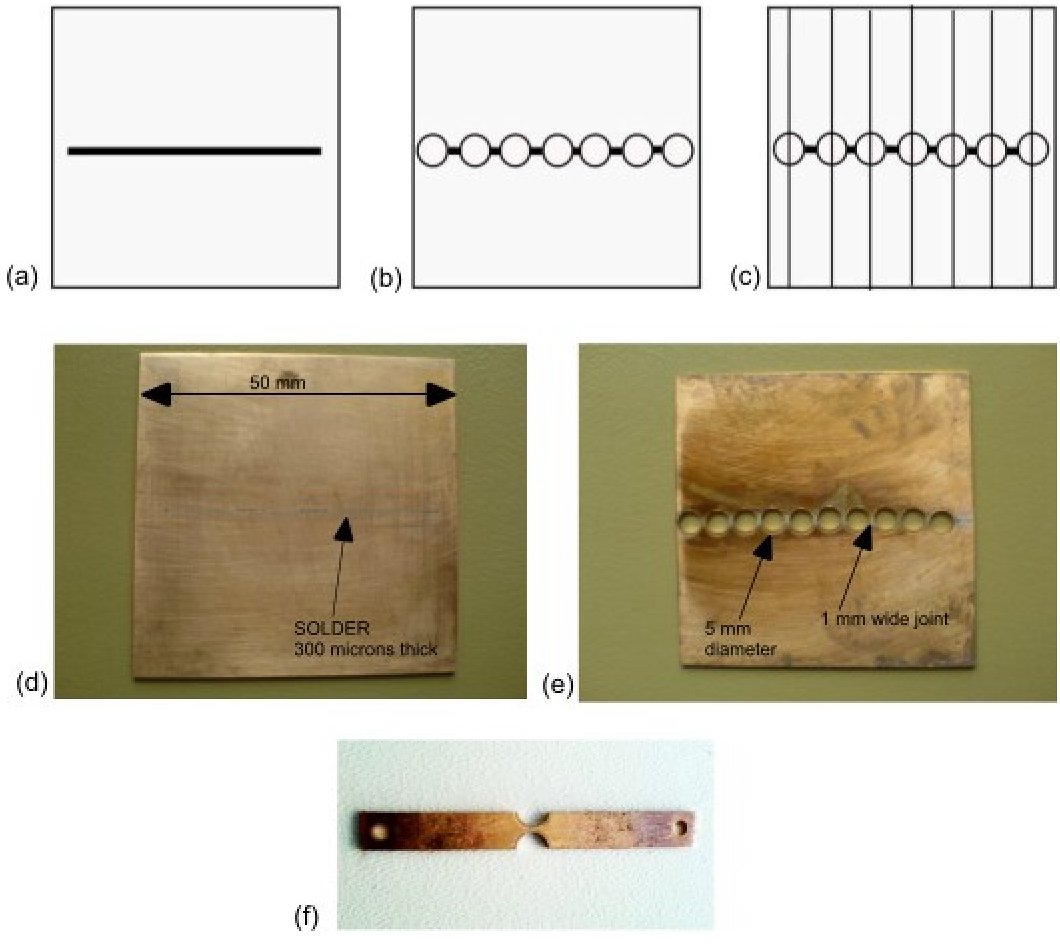

Figure 2: Schematics showing sample preparation (a) The alloy is soldered in the slot. (b) A row of holes is punched. (c) Samples are cut. (d) Photo of the copper plate showing the solder slot. (e) Photo of the solder plate showing the row of holes. (f) Photo of a finished sample.

Historically, the solder joint was universally made using a tin-lead alloy, but today following the introduction of RoHS in July2006, there is a range of lead-free alloys available. However, the resistance of these new alloys to high cycle fatigue under various vibration loads is not fully understood. Hence there is an urgent need for more research to understand the dynamic properties of both traditional and lead-free solders.

Most studies of the effects of vibration on electronic systems have focused [2-8] on full PCBs or ball grid arrays (BGAs). That approach is very useful for studying and qualifying a product, but it does not address directly the materials performance, and hence it is difficult to quantify the impact of changing the alloy in specific terms. The work reported here was aimed at studying the solder alloy performance under high-cycle fatigue by removing the variability introduced by the circuit design and the range of materials used in that construction. This work introduces a methodology that characterises the solder properties by testing a single "model" joint.

2 METHODOLOGY

2.1 Sample Preparation

The samples for this research were prepared from a small copper plate of dimensions 50x50 mm (see Figure 2). A 300 µm slot was cut in the middle of the plate, using a diamond saw, but 1mm was left at either end to ensure that the plate remained as a single piece. The copper plate was then cleaned using isopropyl alcohol and dried using compressed air.

Solder paste was placed in the slot using a syringe, and a small butane gas torch was used to heat the copper to above the solder melting temperature. As the solder paste melted more solder paste was added to the slot to ensure adequate filling. The plate was allowed to cool naturally to ambient temperature, and any excess solder was removed by manually grinding both sides with silicon carbide paper (500 and 1200 grit) until both surfaces were flat. A row of holes (5 mm diameter) was punched along the axis of the solder filled slot, with the holes 3.25 mm apart. Multiple test sample were cut using a diamond saw, with the cut passing through the centre of each hole, in order to form dog-bone style samples. Holes were punched at each end of the cut samples to facilitate fixing in the test rig. The whole sample manufacturing process is highlighted in Figure 2.

2.2 Materials

Samples were prepared with four alloys: Sn60.0%Pb40.0% eutectic, Sn99.2%Ag0.3%Cu0.5% (SAC0305), Sn96.5%Ag3.0%Cu0.5% (SAC305), Sn95.6Ag3.7%Cu0.7% (SAC387). The conventional SnPb alloy was included with the lead-free alloys (a) as a benchmark, and (b) because some high reliability applications are not subject to the ban on lead and continue to use SnPb solder. The other alloys used were commercial lead-free SAC alloys, with different amounts of silver and copper. A fifth set of samples of SAC305 was prepared by annealing at 125^{O}C for 2 weeks. The SAC0305 alloy used here was a commercial alloy with less than 1% silver. The approximate compositions of the alloys are shown in Table **1**.

Table 1: Materials used.

MATERIAL	COMPOSITION
SnPb	Sn 60%, Pb 40%
SAC305[1]	Sn 96.5%, Ag 3.0 %, Cu 0.5%
SAC305A	Sn 96.5%, Ag 3.0, % Cu 0.5%, annealed @125^{O}C , 2 weeks
SAC387	Sn 95.6, Ag 3.7%, Cu 0.7%
SAC0305	Sn 99.2%, Ag 0.3%, Cu 0.5%

2.3 VIBRATION EQUIPMENT

The equipment was built around two piezoelectric actuators, supplied form Physical Electronics, PI P-842.20 [10]. The technical specification of these actuators is given in Table **2**; and a schematic is shown in Figure 3. Each actuator consists of a friction-free, preloaded, monolithic multilayer piezoceramic stack, protected by a stainless steel case. They were chosen because they can operate in the frequency range required by this test, and achieve a relatively large range of travel, 30 μm.

Table 2: Piezoelectric actuator PI P-842.20.

P-842.20	
Travel range (open-loop) for 0 to 100 V (μm) ±20%	15
Resolution closed-loop / open-loop [nm]	- / 0.3
Static large-signal stiffness [N/μm] ±20%	27
Push/pull force capacity [N]	800/300
Electrical capacitance [μF]	3.0
Dynamic operating current coefficient [μA/(Hz × μm)]	12.5
Resonant Frequency [kHz] ±20%	14
Weight without cable [g] ±5%	42
Length [mm]	55

1 For commercial reasons the name and composition of this alloy are not available.

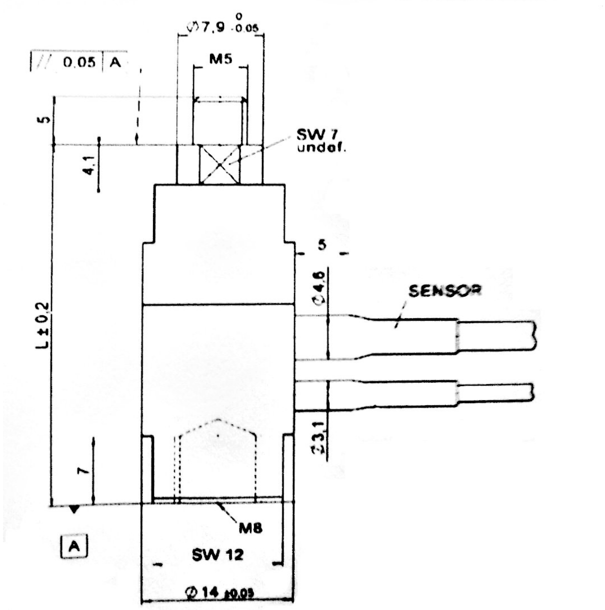

Figure 3: Schematic of the piezoelectric actuator.

Each sample was placed between the two actuators, as shown in Figure 4. The arrangement was based around a vertical axis with the top actuator screwed to a steel plate and driven by an electrical signal to generate the vibration. The second actuator was used to sense the magnitude of the vibration since it was coupled to the first actuator through the sample. The mass of this oscillating second actuator increased the force acting on the sample. Hence, the sample oscillated in the vertical axis driven by the top actuator, and the weight of the second actuator simply added to the force acting on the sample. A simple steel coupling was made to connect the samples to the actuators.

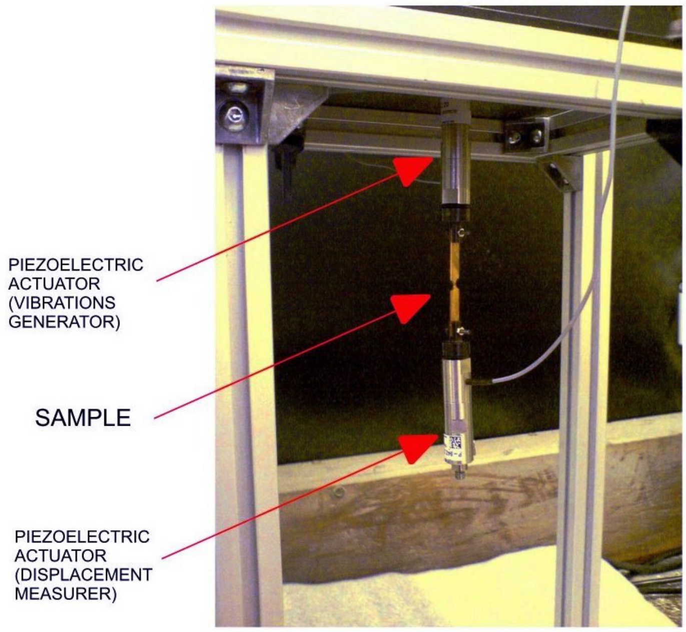

Figure 4: Experimental setup of the actuators and the sample.

2.4 WORKING PRINCIPLE

A wave generator (Agilent 33120A) was programmed to generate a sinusoidal wave with an amplitude of 5V at the desired frequency. A floating power supply (ISO TECH IPS-2010) was used to offset the null position, so that the oscillation could be of equal magnitude around the null point. (Typically, piezoelectric devices only operate in the compression mode, but these devices can support small tensile forces, and by offsetting the null point a symmetrical waveform could be imposed on the sample). This offset sinusoidal waveform was finally amplified using a PI LVPZT amplifier. The top piezoelectric actuator (active piezo) was fed with this periodic voltage, which generated the required displacement and acceleration. The acceleration was a function of the displacement and of the total attached mass of the sample and sense actuator to create the force acting on the solder joint. As the mass is constant, this force changes only with the acceleration from the driven actuator.

The supplied and measured waveform were recorded using an Agilent 54624A oscilloscope. The displacement of the sense actuator depended on the material response of the sample to the applied vibration. This response was observed on a second channel of the oscilloscope to which a computer was connected to record the voltage amplitude as a function of time. The complete experimental arrangement is shown in Figure 5.

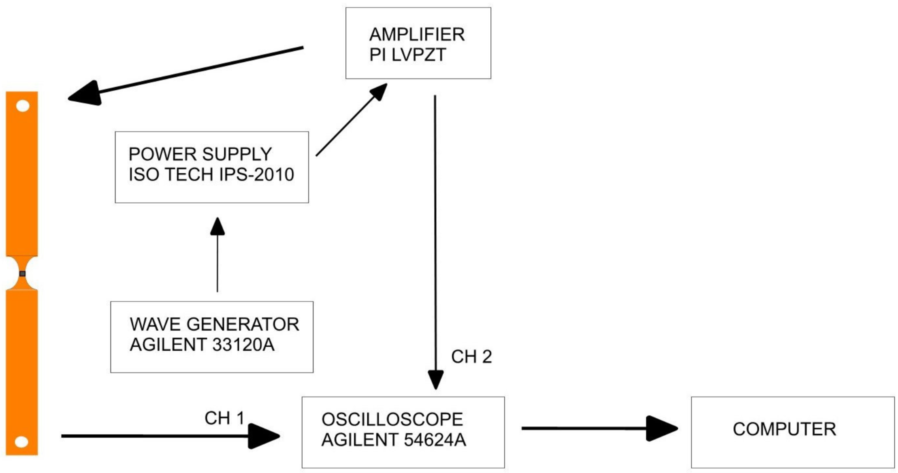

Figure 5: Complete experimental arrangement for vibration testing of solder joints.

2.5 CALIBRATION OF THE SYSTEM

To characterise the acceleration experienced by the sample the voltage output from the sense actuator was quantified by establishing a voltage acceleration calibration curve. The calibration was performed using a laser vibrometer (Polytec MSA-400-PM2-D Micro System Analyser - see Figure 6) to measure the displacement as a function of time. The laser optics of the vibrometer were pointed directly at the sample to measure the sample acceleration. The sample used for the calibration was made of copper only, without the solder described in Section 2.1. This was necessary to avoid the sample rupturing during the calibration process.

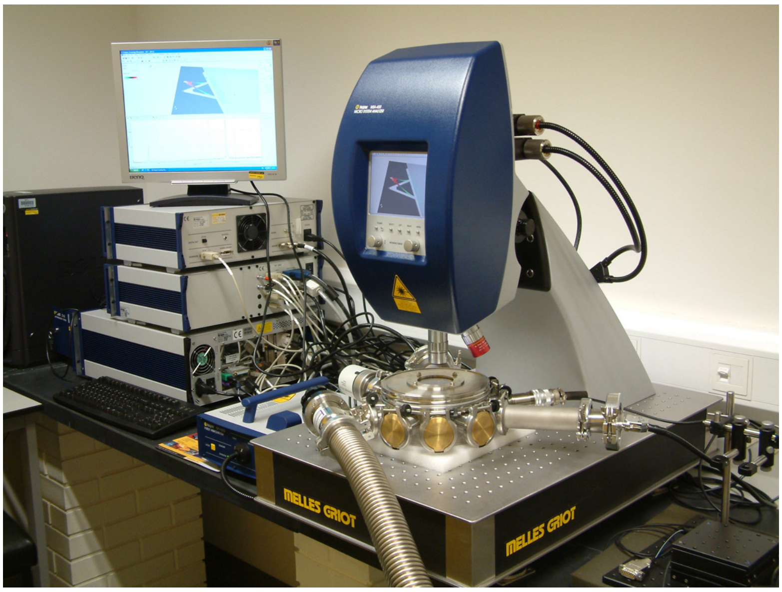

Figure 6: Laser vibrometer used for the calibration of the system.

The acceleration of the sample was measured continuously from 0 to 2 kHz, using five applied voltage amplitudes for the calibration: 100, 200, 500, 2000 and 5000 mV. The results of this calibration process are presented in Figure 7. The acquired data for 2000 and 5000 mV applied voltages stop before reaching 2 kHz; at these conditions, and in the calibration mode, the instrument became too loud to be operated safely.

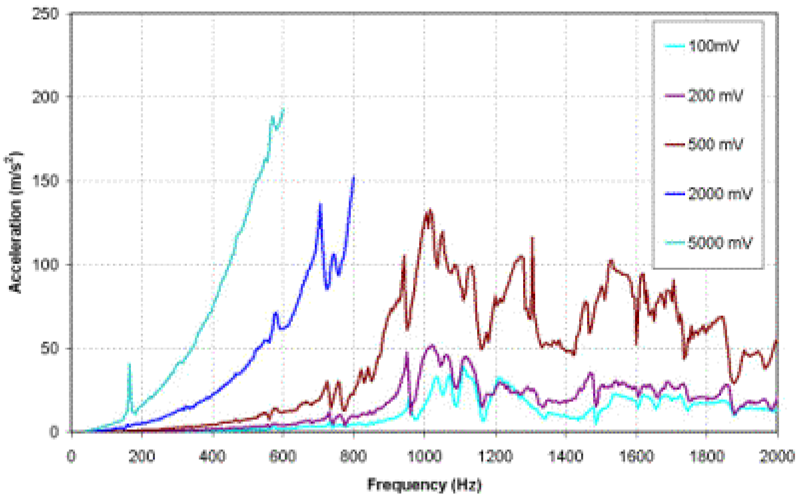

Figure 7: Acceleration response of the copper sample at 5 different voltage amplitudes.

The output voltage amplitude (measured by the sense actuator) was also recorded as a function of frequency for each applied voltage, and these results are shown in Figure 8 for an input voltage of 5 V.

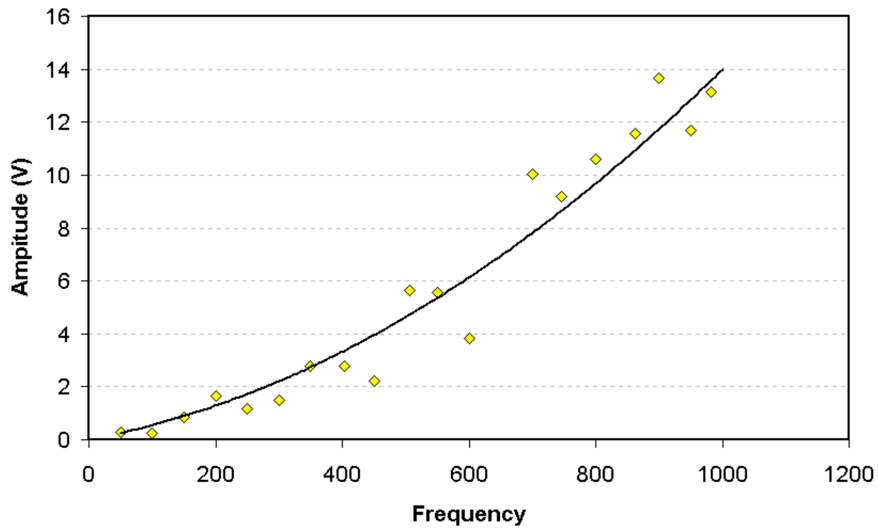

Figure 8: Variation of excitation frequency at 5 V against output voltage amplitude

Finally, the output voltage amplitude was compared with the acceleration of the sample (as measured by the vibrometer, and shown in Figure 7). The calibration graph is presented in Figure 9 and the relation is given by equation 1, where g is the acceleration (in units of acceleration due to gravity, i.e. 9.8m/s) and *v* is the output voltage amplitude.

$$g = -0.206v^2 + 4.771v \qquad (1)$$

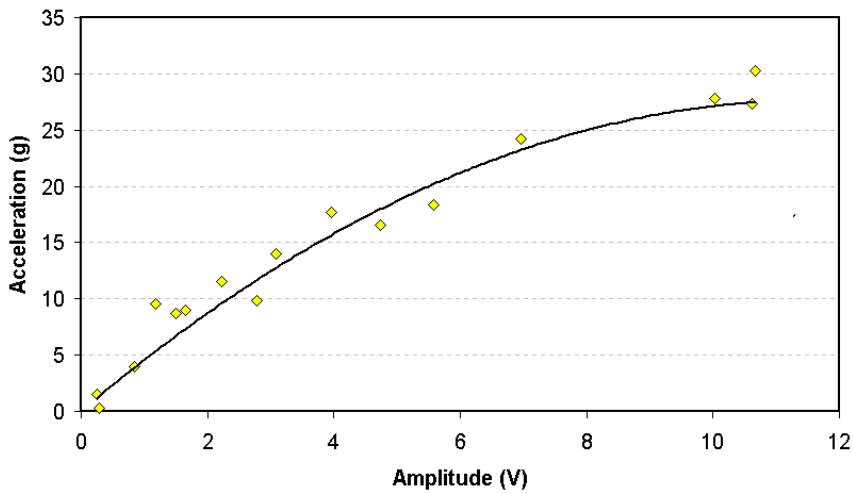

Figure 9: Variation of output voltage amplitude against acceleration (g) of the sample for a range of frequencies.

2.6 EXPERIMENTAL CONDITIONS

Vibration tests were performed using a 5 V amplitude, the value which gave the highest value of acceleration for a given applied frequency (see Figure 7). The calibration data in Figure 8 only go up to 600 Hz for 5V. Two values of frequency were chosen: 400 and 800 Hz, corresponding to acceleration of approximately 10 and 20 g respectively (see Figure 7). The 800 Hz value was chosen for a number of reasons; it is at the upper end for a number of applications, failure is not too rapid for brittle materials, and the noise level was just acceptable. The 400 Hz value was chosen as a more intermediate stress state to study whether the lifetime of the samples changed by halving the frequency and g level. Although the experiments were all conducted at room temperature, in future studies it would be possible to change the design of the equipment so that tests at different temperatures could be performed. The experimental conditions are summarised in Table **3**.

Table 3: Summary of the experimental conditions

	Experimental Conditions
Input Voltage Amplitude	5 V
Frequency	400 Hz, 800 Hz
Temperature	room T
Materials	SnPb, SAC305, SAC387, SAC0307, SAC305 annealed

3 EXPERIMENTAL RESULTS

3.1 SUMMARY OF THE EXPERIMENTAL PROCEDURE

Samples were clamped in the sample holder described in Section 2.3, using screws and nuts. It was of critical importance to proceed carefully in the mounting operation, in order to avoid deformation of the small solder joint and avoid creating defects prior to testing. The sample holder was then attached to the piezoelectric actuators, and data recorded on the system described above. This procedure was repeated for 15 samples in each condition.

3.2 WEIBULL PLOTS

The times to rupture values were used to produce Weibull plots and the results for 400 and 800 Hz are presented in Figures 10 and 11. In the same graphs, the Weibull shape parameter and the characteristic life (or scale) for each material are also indicated. These graphs were produced using the software package Minitab [9]. The results for the annealed SAC305 at 800 Hz are not shown because the samples failed too quickly and the lifetime could not be measured with this method.

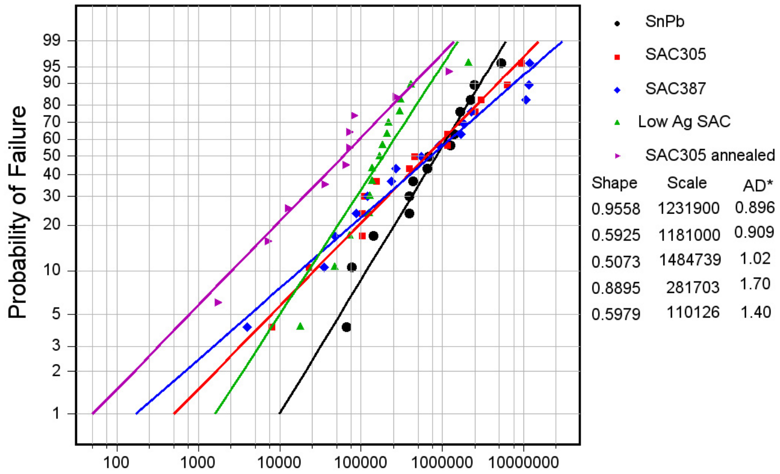

Figure 10: Weibull plot for test at 400 Hz.

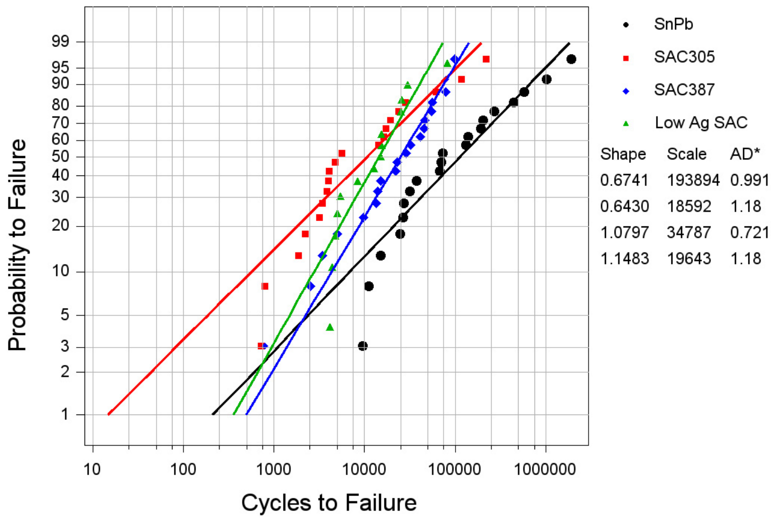

Figure 11: Weibull plot for tests at 800 Hz.

3.3 ACCELERATION PLOTS

The output voltage amplitude for each test was converted into an acceleration using equation 1. The number of vibration cycles for the acceleration levels are illustrated in Figures 12 to 20 for different alloys at the two frequencies. As described above, the acceleration is plotted instead of the force, because the mass is a constant. In each Figure three experimental runs are plotted to indicate the range of the data for each material.

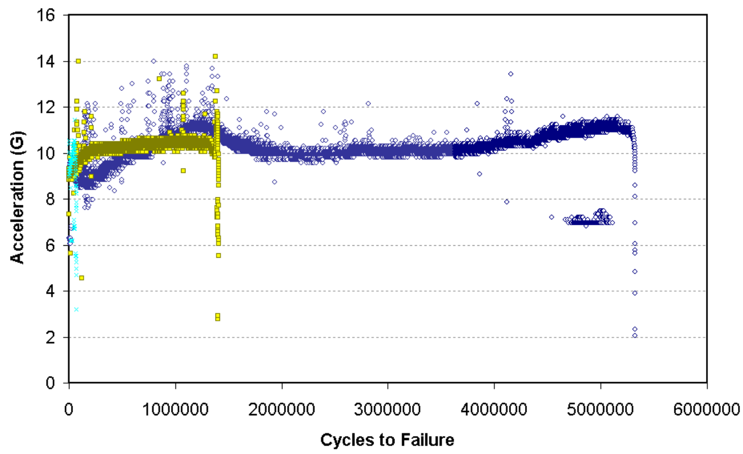

Figure 12: Acceleration plot for Sn-Pb at 400 Hz.

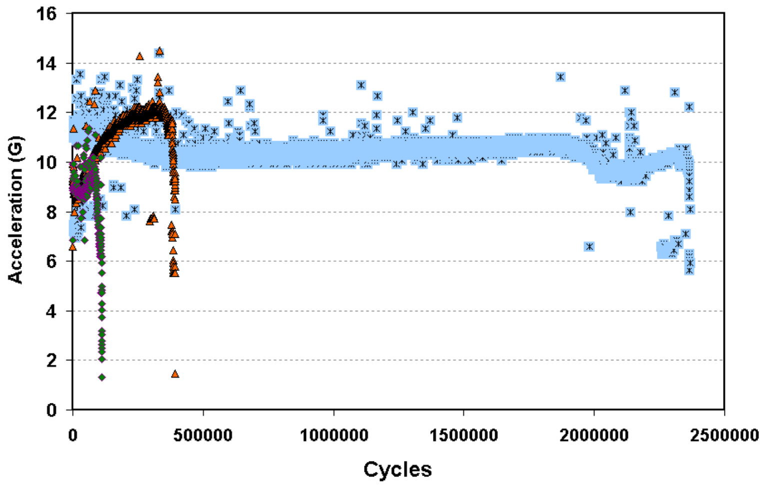

Figure 13: Acceleration plot for SAC305 at 400 Hz.

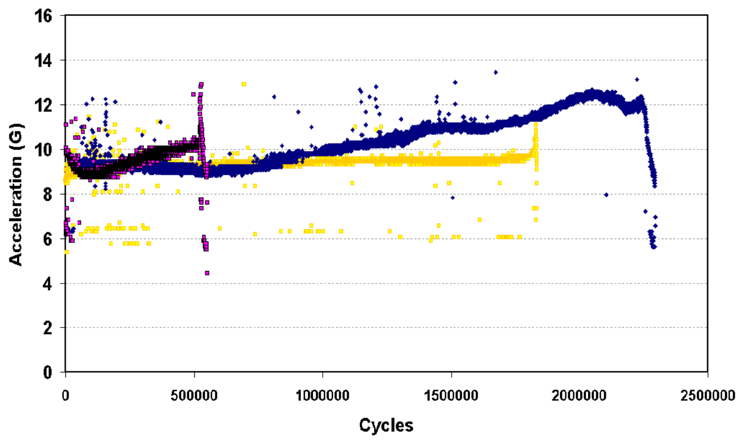

Figure 14: Acceleration plot for SAC387 at 400 Hz.

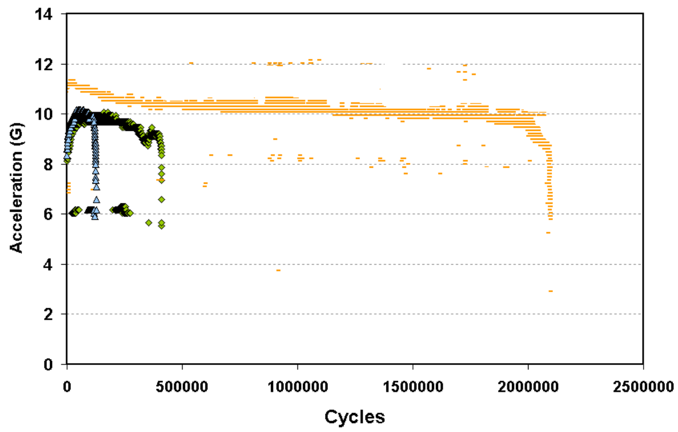

Figure 15: Acceleration plot for the SAC0307 alloy at 400 Hz.

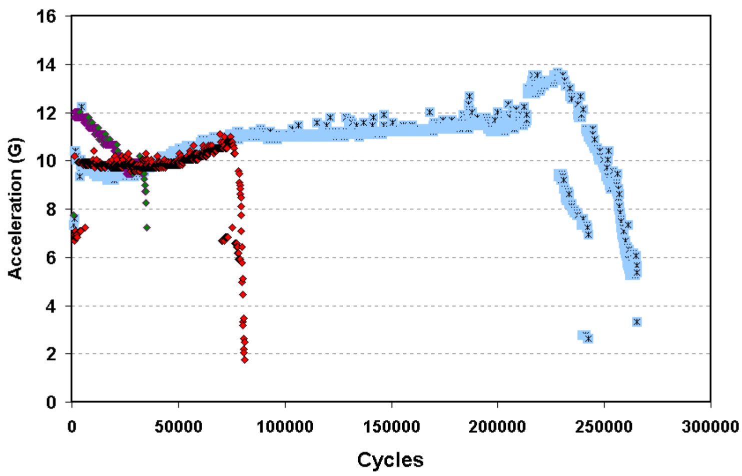

Figure 16: Acceleration plot for the annealed SAC305 alloy at 400 Hz.

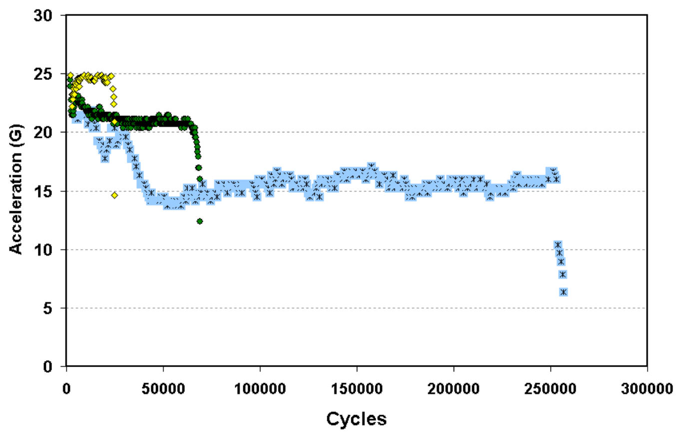

Figure 17: Acceleration plot for the SnPb alloy at 800 Hz.

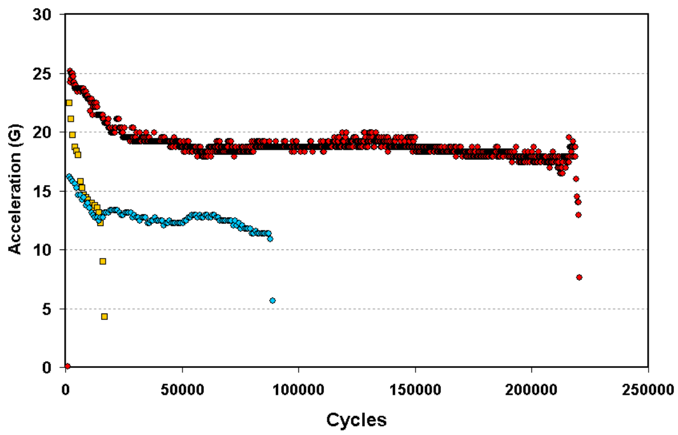

Figure 18: Acceleration plot for the SAC305 alloy at 800 Hz.

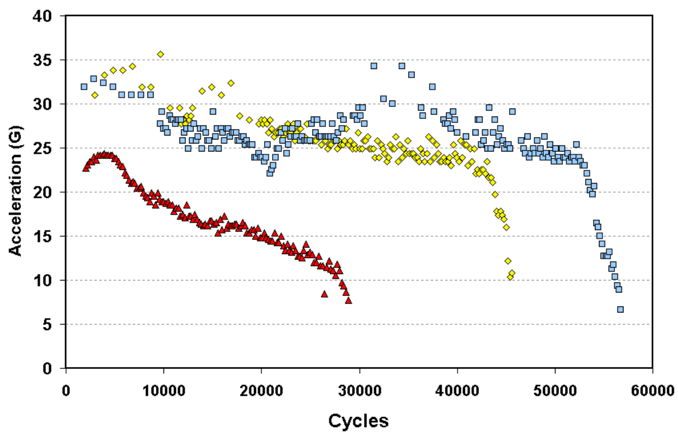

Figure 19: Acceleration plot for the SAC387 alloy at 800 Hz.

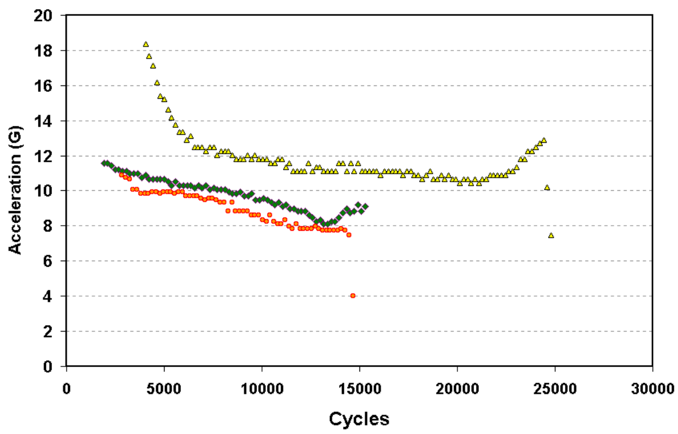

Figure 20: Acceleration plot for the SAC0307 alloy at 400 Hz.

3.4 FRACTURE SURFACE MICROGRAPHS

Typical SEM micrographs of the fracture surfaces from the test samples are presented in Figures 21 to 30. The surfaces were examined from the top and at a tilt of 40°.

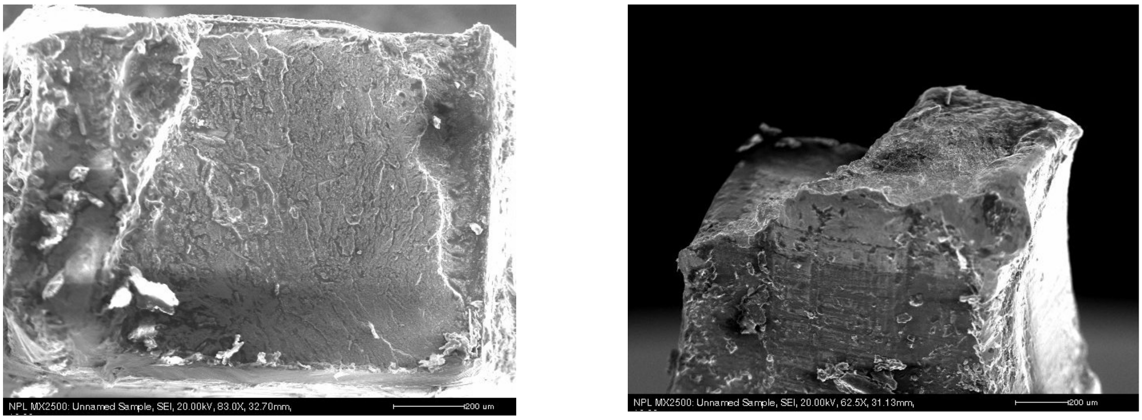

Figure 21: SnPb, 400 Hz

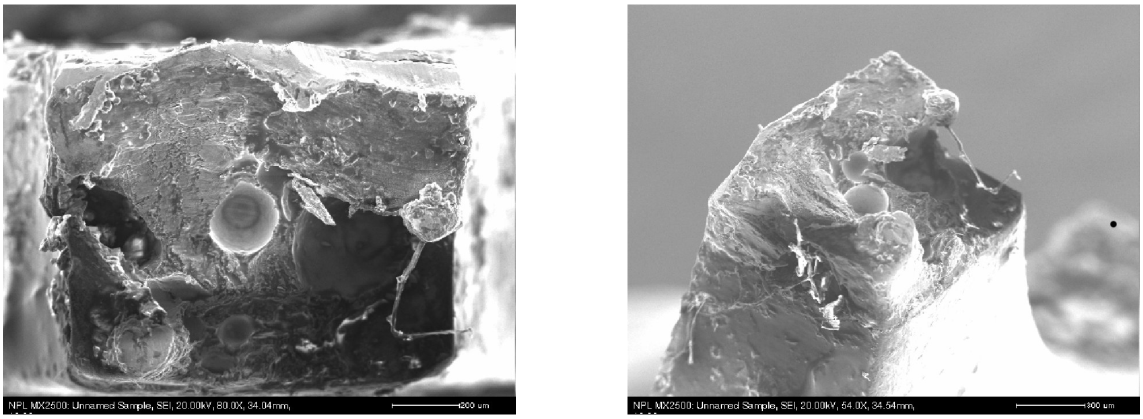

Figure 22: SAC305, 400 Hz

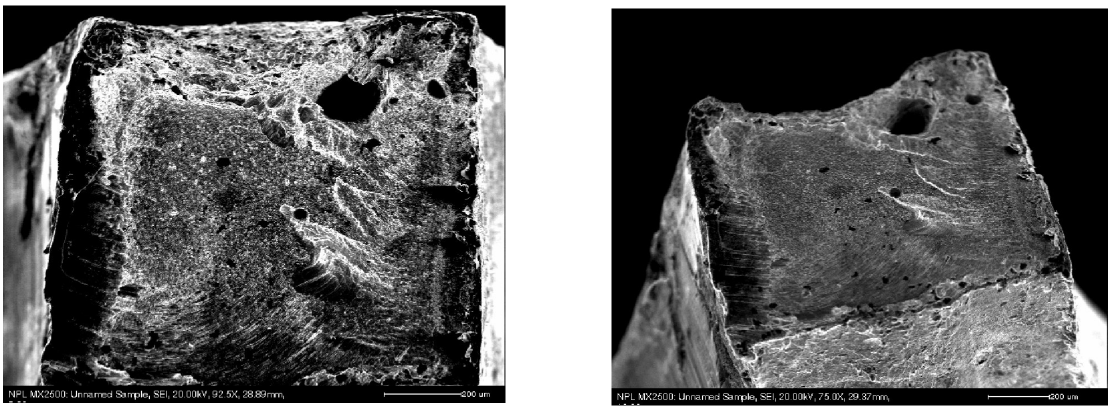

Figure 23: SAC305, annealed, 400 Hz

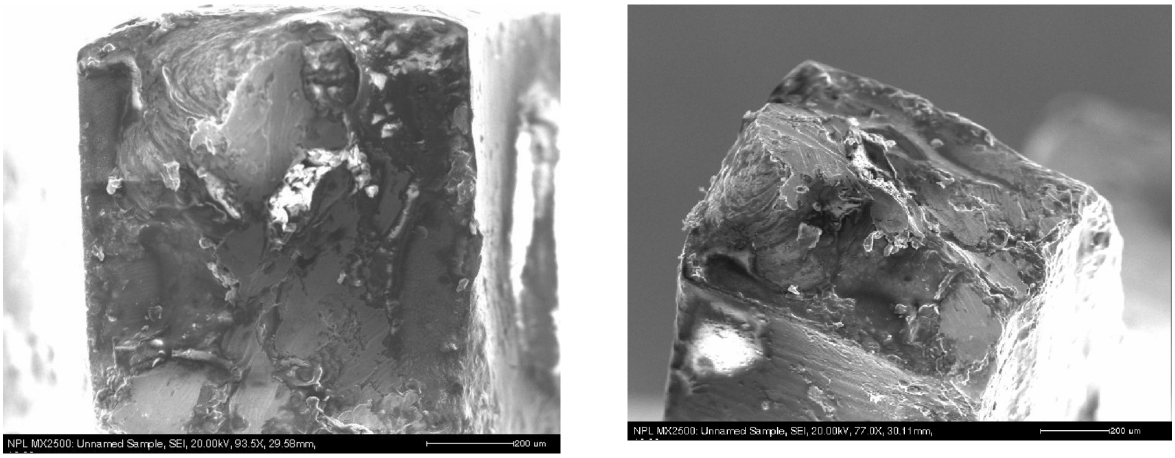

Figure 24: SAC387, 400 Hz

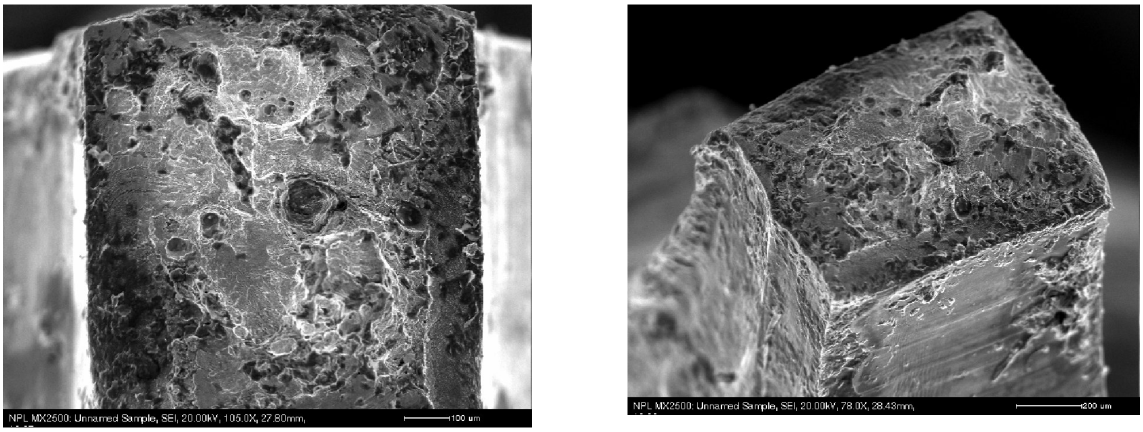

Figure 25: SAC0307, 400 Hz

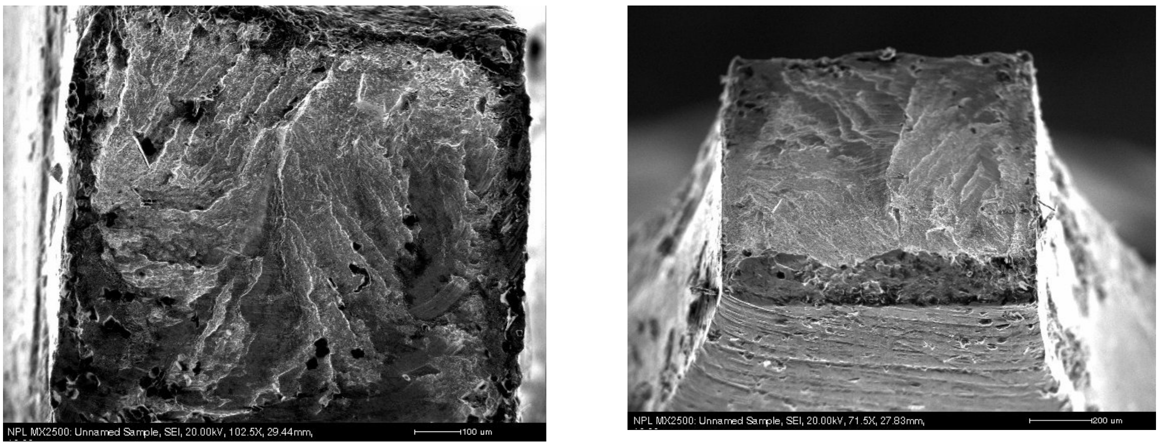

Figure 26: SnPb, 800 Hz

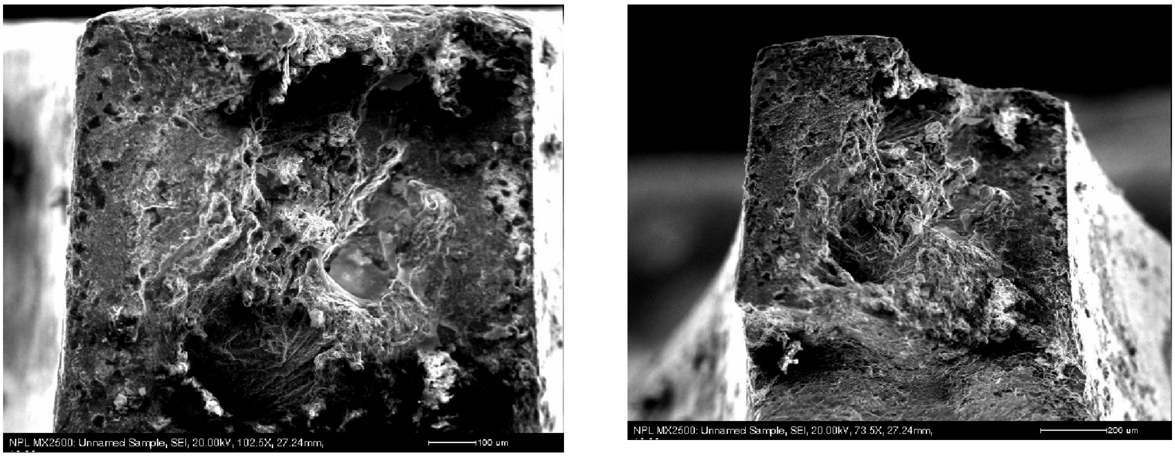

Figure 27: SAC305, 800 Hz

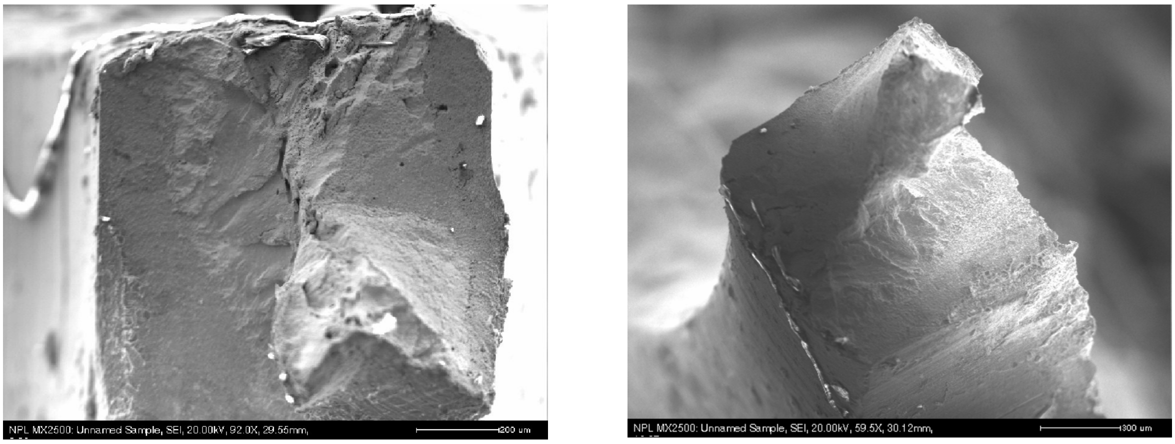

Figure 28: SAC305, annealed, 800 Hz

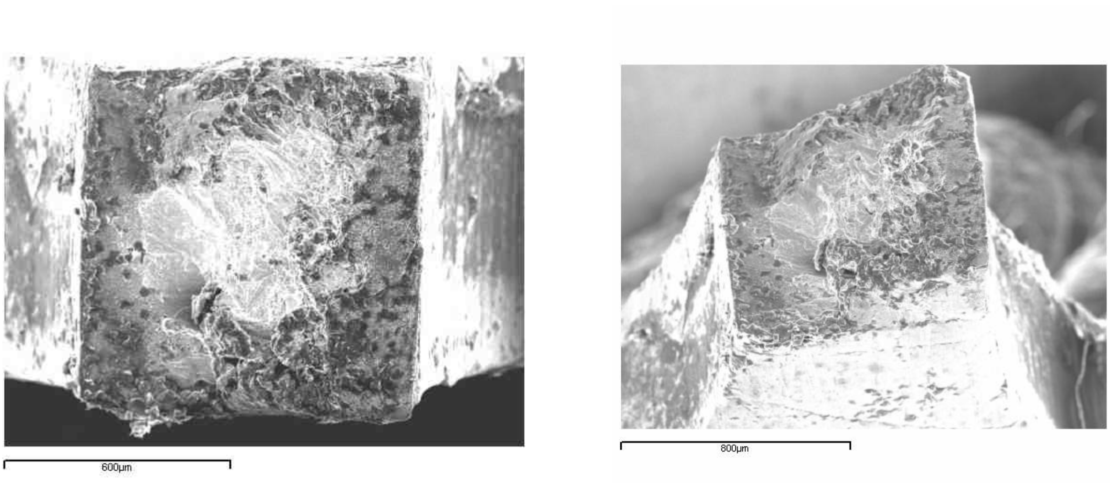

Figure 29: SAC387, 800 Hz

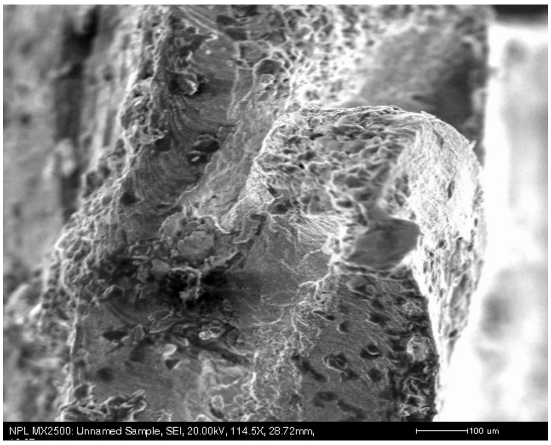

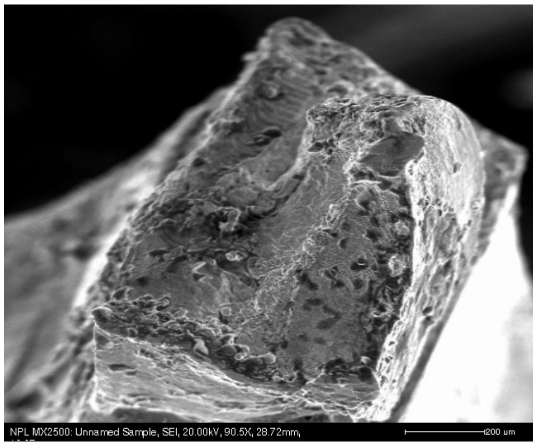

Figure 30: SAC0307, 800 Hz

3.5 MICROGRAPHS OF CROSS-SECTIONS

Samples that were photographed for the fracture surface analysis, were also cross-sectioned, ground and polished to a final grade of 1 mm diamond paste. Secondary electron SEM micrographs of these cross-sections are illustrated in Figure 31.

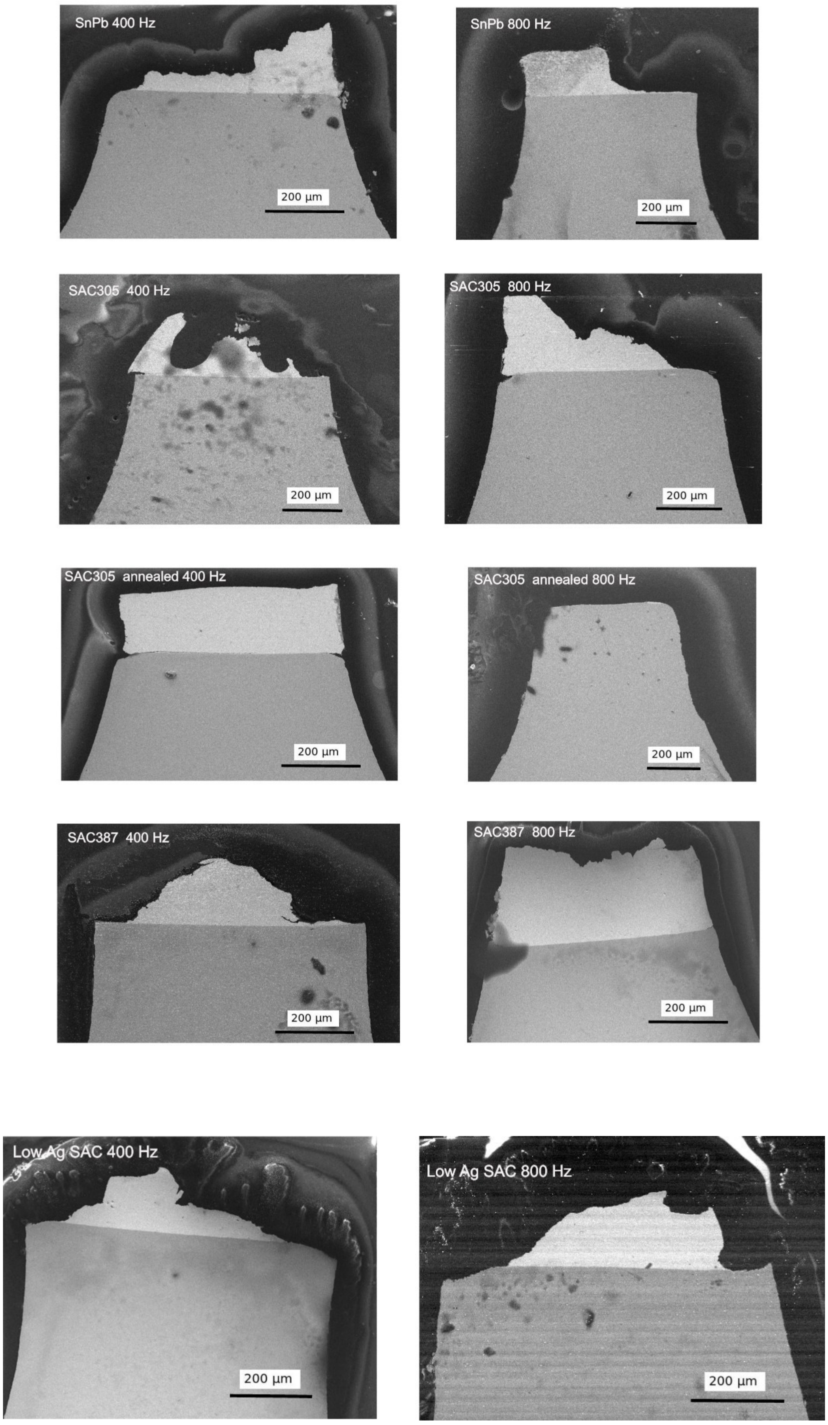

Figure 31: SEM micrographs of cross-sections of broken joints.

4 DISCUSSION

4.1 DISCUSSION ABOUT WEIBULL PLOTS

The Weibull diagrams in Figures 10 and 11 show a clear difference in lifetime resistance between the various materials. At 400 Hz, the shape parameter (normally called β) is <1 for all materials. As β becomes smaller there is an increase in the failure rate at a lower number of cycles, and hence these materials accumulate more failures initially. The lower β also indicates that there could be more than one operative failure mechanism.

The early failures of the SAC alloys maybe attributed to two main factors: microstructure propensity to brittle failure, and latent defects. SnPb alloy has $\beta \approx 1$, indicating a more constant failure rate and predictable behaviour. The Weibull characteristic life (normally called alpha) shows that the best performing materials at 400 Hz are SAC387 and SnPb, whilst the worse is the annealed SAC305. The improving performance from low silver to SAC305 and SAC387, seems to indicate that *the presence of silver has a favourable effect on the high-cycle fatigue of lead-free alloys*. This trend is highlighted in Figure 32.

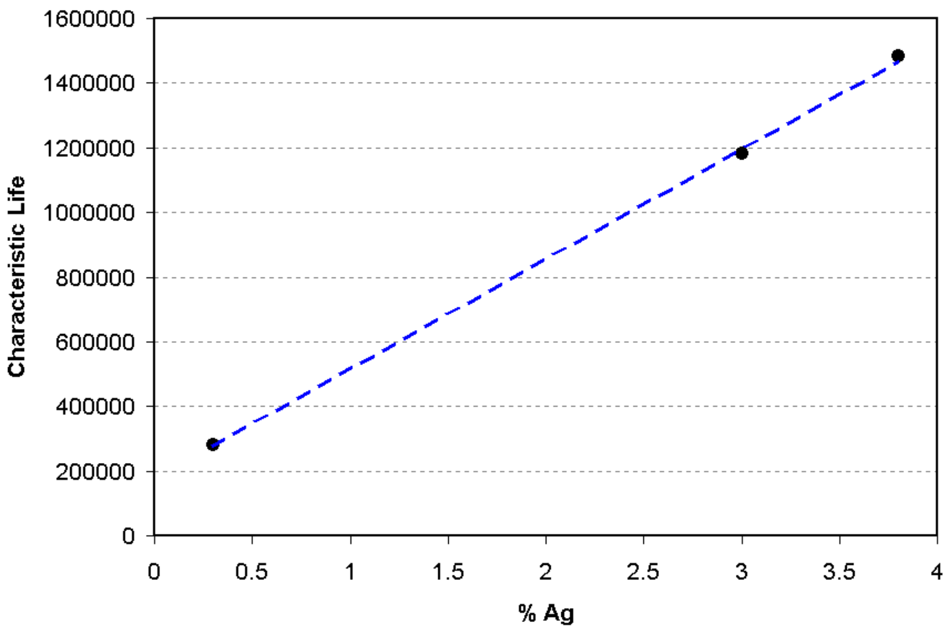

Figure 32: % silver in the alloy against Weibull characteristic life at 400 Hz.

On increasing the frequency to 800 Hz the situation changes. In this case $\beta<1$ for SnPb and SAC305, and it is $\beta \approx 1$ for SAC387 and low Ag, indicating that these last two materials have the most consistent behaviour. The characteristic life shows that the best performer is again SnPb. As noted above the annealed SAC305 failed too quickly to be detected by the instrumentation. A performance comparison between the 400 Hz and 800 Hz data is presented in Figure 33. The effect of the increased frequency and acceleration on the lifetime of the samples is clear. The characteristic life decreases at 800 Hz by an order of magnitude for the SnPb and low Ag alloy and by more for the SAC305and SAC387 alloys. It is also interesting to note that there is a significant change in β for the SAC387, indicating a change in the failure mechanism.

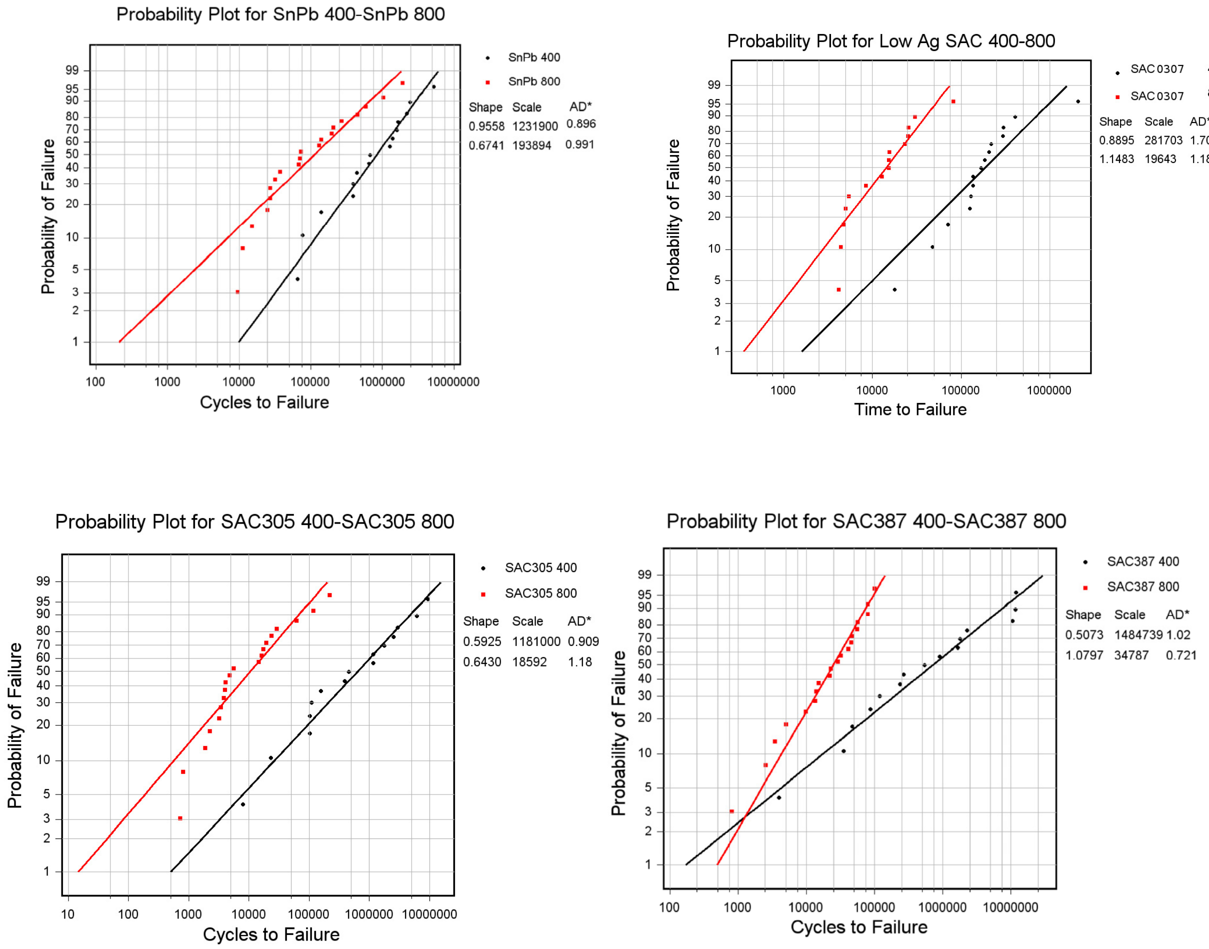

Figure 33: Weibull plots for SnPb, SAC0307, SAC 305 and SAC387 at 400 and 800 Hz

4.2 DISCUSSION ABOUT THE ACCELERATION PLOTS

The acceleration plots presented in Figures 12 to 20 show the instantaneous response from all the tests of the samples to the applied vibration. No clear differences were apparent for the various materials. However, a general behaviour for each frequency could be identified. This behaviour consisted of three phases, which are summarised in Figure 34 at 400 and 800 Hz.

At 400 Hz, the first peak corresponds to strain hardening and crack formation. The second stage is probably due to high-cycle fatigue and the slow propagation of the crack. During this stage the material has time to further strain-harden; in fact the slope of the curve is positive. In the third stage the crack has grown to an extent that the sample is only supported by a small remaining area, and then heavy plastic deformation occurs to fracture. At 800 Hz the first stage is again likely to correspond to a strain hardening phase. At this frequency the second phase displays a negative slope. This is probably due to a faster fatigue process and increased crack propagation with no strain hardening occurring, and might be one of the reasons why samples failed much earlier at 800 Hz than at 400 Hz. The third stage was once again similar to that observed at 400 Hz.

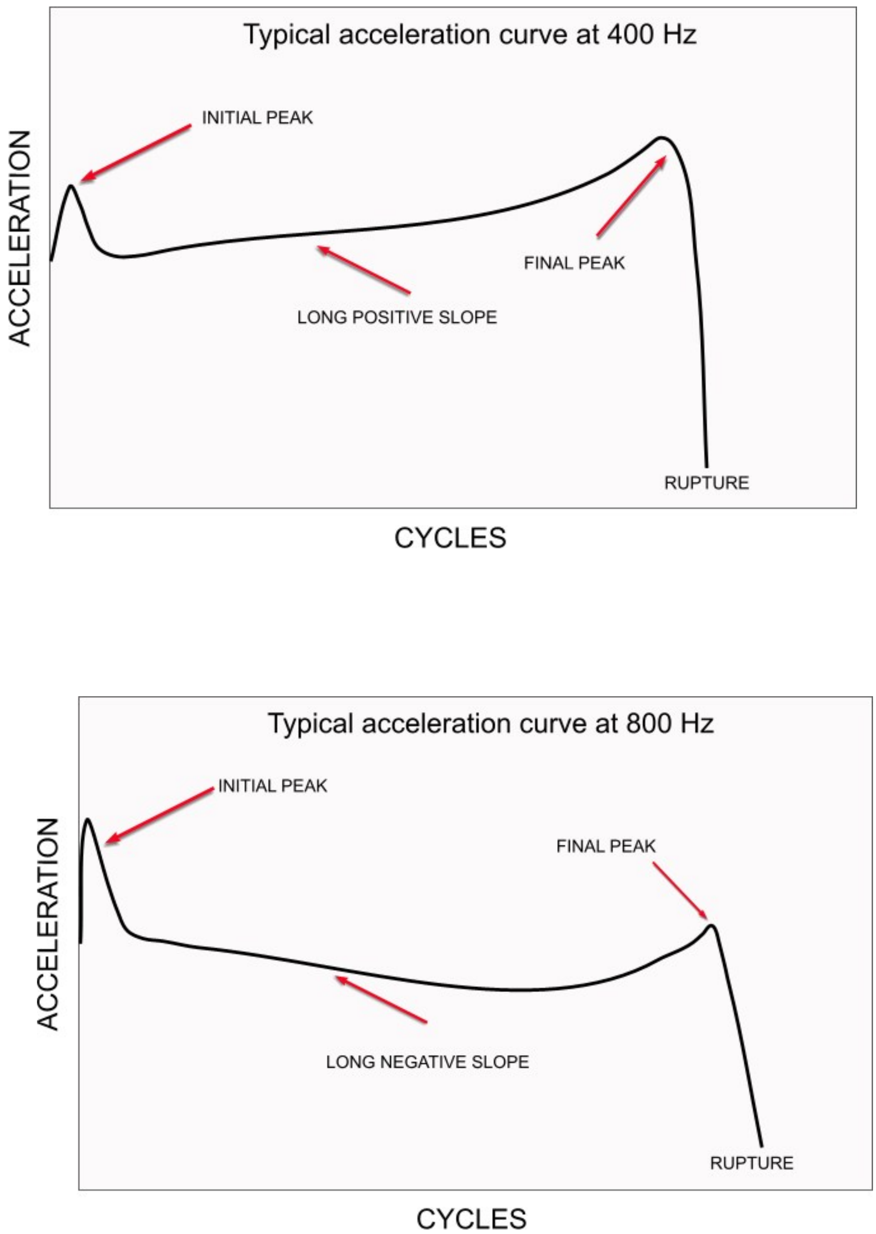

Figure 34: Typical acceleration curves for solder alloys vibrated at 400 and 800 Hz.

4.3 DISCUSSION ABOUT THE FRACTURE SURFACES

From the fracture surface images presented in Figures 21 to 30 it was observed that:

- SnPb fracture surfaces look more "homogeneous" (see Figures 21 and 26).
- SAC305 fracture surfaces are more "irregular" - a large number of voids and fractures can be seen in Figures 22 and 18. Voids reduce the solder cross-sectional area, and could be one of the reasons for the poorer performance of this material compared to SnPb.
- Fractures do not produce a flat surface (apart from a few cases e.g. in Figures 23 and 25).
- Fatigue striations were observed (see Figures 22 and 35).
- Some striations due to twisting of the samples were also observed (see Figures 24 and 35). Twisting probably occurs before rupture, when fracture has propagated across almost the whole section. At that point it is likely that the samples will vibrate in different modes, including twisting.
- Signs of ductile fracture (see Figure 35) were observed in almost all samples apart from the annealed alloy.

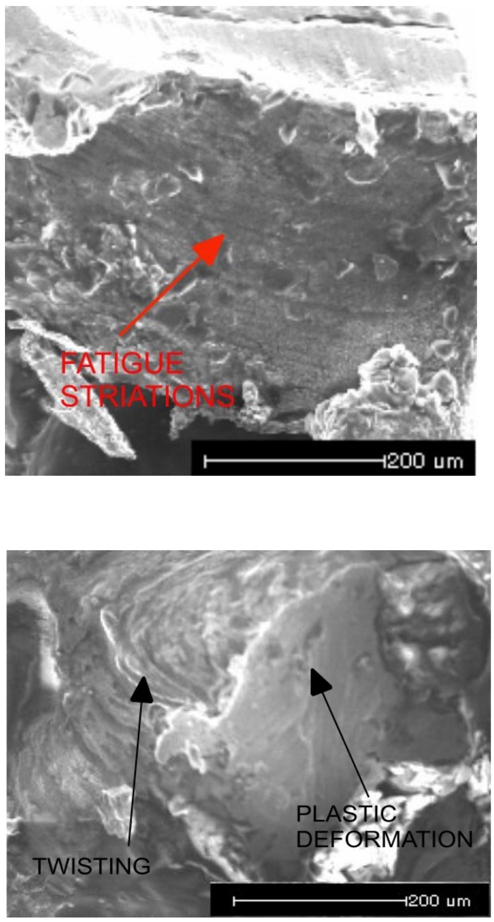

Figure 35: (a) Fatigue striations on a SAC305 sample (400Hz),
(b) signs of twisting and plastic deformation.

4.4 DISCUSSION ABOUT THE CROSS-SECTIONS

From the cross-sections of broken samples shown in Figure 31 the following observations can be made:

- In a few cases the fracture surface appeared non-planar (SAC 305 annealed, SAC 387 at 800Hz). Some fractures appeared to run at 45°, an indication that the fracture was partly ductile. These results, however, cannot be taken as conclusive, because not all 15 samples for each material and at each frequency were analysed, and hence there is not enough statistical evidence to confirm these observations.
- Fracture was very close to, if not at, the intermetallic/solder interface. The intermetallic layer, however, was not removed completely from the copper. An example of this behaviour is given in Figure 36 and this micograph supports the view that the fracture propagates at the intermetallic interface. However, more research is needed to confirm this suggestion..

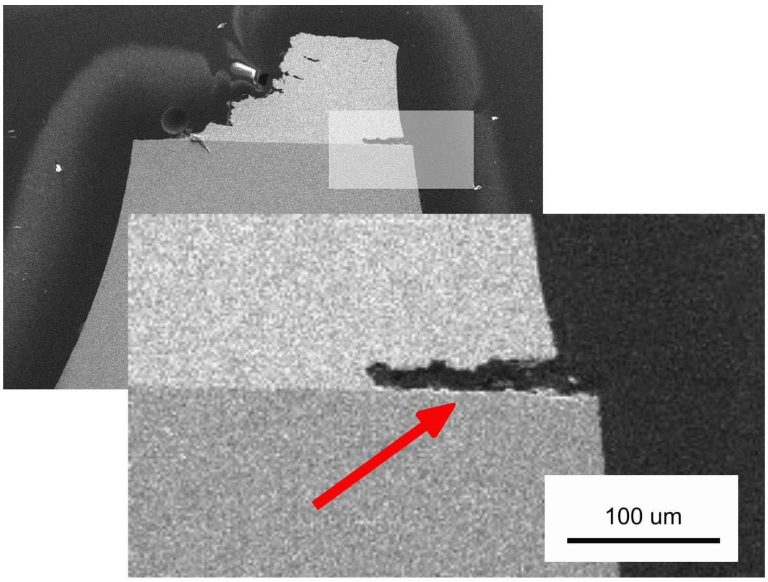

Figure 36: SEM image of a crack on the interface on a SAC305 sampled vibrated at 800 Hz.

- The SAC305 annealed sample had a planar fracture surface running near the intermetallic layer. This is an indication of brittle fracture and could explain the poor behaviour of this material at 400 and 800 Hz.

The intermetallic is a higher strength material than either the solder or the copper and it is less likely to undergo plastic deformation. This discontinuity in properties may contribute to a weakness in high cycle fatigue performance and make the role of the intermetallic key in determining the solder joint performance.

5 CONCLUSIONS

High frequency vibration tests have been performed on SnPb, SAC0307, SAC305 and SAC387 solder joints. The main findings are:

- The test method developed here has been demonstrated to be a valuable tool for investigating solder alloy performance subjected to high-frequency vibrations. The equipment is competitively priced (compared to industrial shakers) and flexible enough to be operated at various levels of frequency and acceleration.
- The work has demonstrated that the test method was particularly useful in ranking various alloys in terms of vibration performance. The SnPb alloy was shown to have a better overall performance than lead-free alloys, especially at 800 Hz. These results are consistent with those found in other studies [11].
- The results demonstrate that the higher the concentration of silver in the lead-free alloys the better the performance at 400 Hz. Annealing was found to be deleterious in terms of performance at both 400 and 800 Hz. This effect maybe due to changes in the intermetallic, along which the crack path propagates.
- The lifetime of solder alloys and their relative ranking is frequency-dependent.
- Differences in acceleration graphs showed that different crack propagation modes act at different frequencies. Two main strain-hardening peaks were found from the acceleration plots, one at the beginning of the vibration and one just before fracture. In the intermediate period, further strain hardening was observed at 400 Hz, but not at 800 Hz.
- Fracture surfaces showed many ductile fracture features and fatigue striations. Fracture seems to occur mainly near the intermetallic compound interface, which evidently is the most stressed area. The intermetallic was unaffected by the fracture process, with the crack typically following a path just above it.

ACKNOWLEDGMENTS

The authors would like to thank Milos Dusek for his contribution in the equipment design and for the data acquisition software and Goodrich Engine Control Systems for sharing their experience in the field and the results of their studies. The authors would also like to thank Martin Lowe for help with the vibrometer measurements. The work was carried out as part of a project in the Materials Processing Metrology Programme of the UK Department of Trade and Industry.

REFERENCES

[1] D. S. Steinberg, *Vibration Analysis for Electronic Equipment*, 2000, John Wiley & Sons, Inc

[2] C. R. Siviour, S.M. Walley, W. G. Proud, J. E. Field, *Mechanical Properties of SnPb and lead-free solders at high rates of strain*, J. Phys. D: Appl. Phys. 38 (2005) 4131-4139

[3] JG-PP/JCAA *Lead-Free Solder Projects, Joint Lead-Free Solder Test Program for High Reliability Military and Space Applications*, www.jgpp.com, 2006

[4] Y. Zhao, C. Basaran, A. Cartwright, T. Dishongh, *Thermomechanical Behavior of BGA Solder Joints Under Vibration: An Experimental Observation*, Electronic Packaging Laboratory SUNY at Buffalo, NY

[5] T. A. Woodrow, JCAA/JG-PP *No-Lead Solder Project: Vibration Test*, The Boeing Company, www.jgpp.com, 2006

[6] E. Martynenko, W. Zhou, A. Chudnovsky, R. S. Li, L. Poglitsch, *High Cycle Fatigue Resistance and Reliability Assessment of Flexible Printed Circuitry*, Transactions of the ASME, Vol. 124, 2002

[7] X. Liu, V. K. Sooklal, M. A. Verges, M. C. Larson, *Experimental Study and Life Prediction on High Cycle Vibration Fatigue in BGA Packages*, Microelectronics Reliability, Vol. 46, pages 1128-1138, 2006

[8] Y. Zhao, C. Basaran, A. Cartwright, T. Dishongh, *Thermomechanical behavior of micron scale solder joints under dynamic loads*, Mechanics of Materials, Vol. 32, pages 161-173, 2000

[9] www.minitab.com

[10] PI website, www.pi.ws

[11] N. Barry, I. P. Jones, T. Hirst, I. M. Fox, J. Robins, *A new method for the high-cycle fatigue testing of lead free solder joints*, Goodrich Engine Control Systems/University of Birmingham, IPC/Soldertec Global 4th International Electronics Conference, Malmo, Sweden, April 25-27, 2006